



# EFFECT OF SURFACTANT ON STRUCTURAL, MORPHOLOGICAL, OPTICAL AND ELECTRICAL PROPERTIES OF CUO NANOPARTICLES AND ITS P-N JUNCTION DIODE APPLICATION

D. Selleswari<sup>1</sup>, P. Meena<sup>2</sup>, D. Mangalaraj<sup>3</sup>, G. Jeevitha<sup>4</sup>

<sup>1</sup>PG and Research Department of Physics, Chikkaiah Naicker College, Erode.

<sup>2</sup>Department of Physics, P.S.G.R. Krishnammal College for Women, Coimbatore.

<sup>3,4</sup>Department of Nanoscience and Nanotechnology, Bharathiar University, Coimbatore.

## Abstract

The copper oxide (CuO) nanoparticles (NPs) were prepared simply by Hydrothermal process using various concentration of the surfactant of cetyltrimethyl ammonium bromide (CTAB –0.05 and 0.1 M) and their structural, optical, dc electrical and diode properties have been analyzed. From the XRD analysis, the crystallite size of the CTAB assisted CuO NPs was reduced. The CTAB caused an increase in the optical absorbance and band gap of the NPs. The morphological changes in the sponge, plate like structure under the strong influence of the surfactant were observed from SEM analysis. The FT-IR spectrum confirmed that the presence of Cu and O elements. The dc electrical analysis revealed that conductivity increased while using CTAB. The electrical parameters of ideality factor ( $n$ ), barrier height ( $\Phi_B$ ), series resistance ( $R_s$ ) and interface properties for the n-Si/p-CuO diodes have been analyzed by the I-V method.

**Key words:** Copper oxide, Nano particles, Hydro thermal, Diode.

## 1. Introduction

The metal oxide nanomaterials and nanostructures are under extensive investigation on the researchers owing to their remarkable properties of a higher surface-volume ratio, nanoscale quantum confinement effects and chemical stability. The copper oxide (CuO) is one of the most significant p-type semiconducting metal oxide material with narrow and indirect energy band-gap (1.2-1.8

eV), an outstanding stability, decent optical and electrical properties [1,2]. It has used in the potential applications including gas sensors, batteries, photovoltaics, photo-catalysis and super capacitors [3-7]. CuO nanostructures with dimensionalities (wires, tubes, seeds, belts, sheets rods, leaves, needles and platelets) were synthesized by using polymers, complex agents organic acids, additives and surfactant [8,9]. Significantly, the surfactant is utilized to help the formation of nanoscale materials with modifying the ensuing morphologies and its impact on morphology and physical properties of the materials. The CTAB is widely used to form various nanostructure in the metal oxides. Zou et al. [10] reported the cationic surfactant CTAB assisted flower-like nanocrystalline CuO was prepared by hydrothermal method. Reddy et al. prepared flake-shaped CuO nanostructures by in a co-precipitation method [11]. CTAB assisted CuO hollow microspheres have prepared through via simple hydrothermal method by Wang et al [12]. CuO nanostructures prepared by various preparation methods such as co-precipitation, sol-gel, solvo-thermal reactions, hydrothermal method [13-16]. Among them, Hydrothermal process is the cost effectively, easy process to prepare the various types of nanostructures [17].

In this work, the CuO NPs were prepared simply by Hydrothermal process using various concentration of the CTAB. The structural, optical and dc electrical and diode properties have been analyzed.

## 2. Experimental techniques

The Hydrothermal method was used to synthesizing the CuO NPs. The copper acetate monohydrate ( $\text{Cu}_2(\text{OAc})_4(\text{H}_2\text{O})_2$ ) used as source material of the Cu. The mixture of 0.1 M of the  $\text{Cu}_2(\text{OAc})_4(\text{H}_2\text{O})_2 \cdot 2\text{H}_2\text{O}$  was dissolved in the 50 ml of water and it is stirred at room temperature. After 10 mins, 0.05 and 0.1 M of CTAB were added the in the solution. The PH of the solution was increased by adding NaOH till the solution attains the PH level of 10. After stirring for 1hr, the prepared solution was filtered to the autoclave and maintained the temperature the temperature 150°C for 5 hrs in hot oven. Finally, the resulting power was collected and dried at 60 °C for 4 hrs as for removing organic templates in a vacuum oven.

### 2.1 Fabrication of p-CuO/n-Si heterostructures

The n-type silicon (Si) wafer is used to formation of p-n junction diode. The Si wafer is cleaned well using piranha solution ( $\text{H}_2\text{SO}_4:\text{H}_2\text{O}_2$ ) in the ratio of 3:1 for to remove impurities.

## 3. Results and discussion

### 3.1 X-ray diffraction analysis

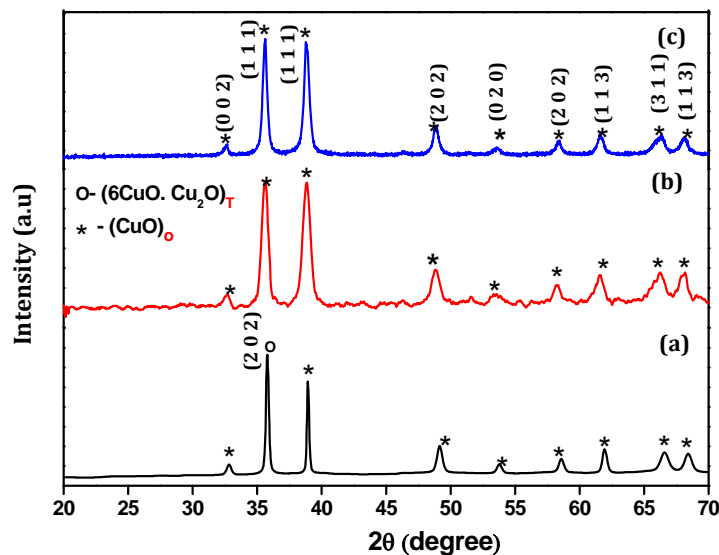


**Fig. 1(a-c)** XRD spectrum of the CTAB assisted CuO NPs, (a) pure CuO NPs, (b) 0.05 M of CTAB:CuO NPs and (c) 0.1 M of CTAB:CuO NPs.

From the figure 1(a)-(c), X-ray diffraction pattern of the pure and CTAB assisted CuO NPs. The Fig. 1(a) observed that the mixed crystal phases of CuO with orthorhombic and tetragonal structure on the basis of JCPDS Card No. 65-2309(o-6CuO.  $\text{Cu}_2\text{O}$ ) and (t-CuO) data. It is seen that the prominent peak of the 32.84 with the (h k l) value is (2 0 2) is referred orthorhombic crystal structure for 6CuO.  $\text{Cu}_2\text{O}$

Hereafter, the  $\text{H}_2\text{O}:\text{HF}$  solution in the ratio of 10:1 is used for remove the native oxides from the Si wafer. The prepared colloidal Hydrothermal was coated on the n-type Si wafer. After completing coating process, the top electrode of the silver paste the silver (Ag) paste was applied on the both surfaces of p-CuO/n-Si junction diode for better contacts.

### 2.2 Characterization techniques

The structural analysis of the CuO NPs was obtained using an powder X-ray diffractometer of the X'PERT-PRO with the radiation source of  $\text{CuK}\alpha_1$  with the wavelength of ( $\lambda$ ) 1.5406 Å. The optical properties of the prepared CuO NPs were analyzed by Perkin Elmer Lambda 35 UV-visible spectrophotometer in DRS method. The electrical analysis of the CuO NPs was measured by Keithley 6517-B electrometer in the temperature from 29 °C to 100 °C at 25 °C intervals. Also, the I-V characteristics of the p-CuO/n-Si junction diode were analyzed using Keithley 6517-B electrometer in the dark.

phase, while remaining peaks of 38.91, 49.11, 53.79, 58.62, 61.86, 66.43 with (h k l) values are (1 1 1), (1 1 1), (2 0 2), (0 2 0), (2 0 2), (1 1 3), (3 1 1), (1 1 3), respectively is referred as tetragonal crystal structure of CuO phase. This indicates that the CTAB influences on the crystal structure of the CuO phase.

The average crystallite (D) size of the pure and CTAB assisted CuO NPs was calculated using the Debye-Scherrer's formula

$$D = \frac{0.89 \lambda}{\beta \cos \theta} \quad (1)$$

where D is the crystallite size,  $\lambda$  is the wavelength for  $\text{CuK}\alpha_1$  source,  $\beta$  is the full width half maximum of a diffraction peak and  $\theta$  is the diffraction angle in degrees. The average crystallite size of without surfactant CuO film is

25.02 nm and CTAB assisted CuO NPs decreases the D value of 13.23 and 17.99 nm for 0.05 and 0.01 M of CTAB, respectively. The low D value is observed for 0.05 M CTAB assisted CuO NPs.

The dislocation density ( $\delta$ ), micro strain ( $\epsilon$ ) and stacking fault (SF) values are calculated by the following equations (2-4). The calculated parameters were listed in the **table 1**.

**Table 1:** structural parameters of the CTAB assisted CuO NPs.

CuO NPs with CTAB in wt. %	2 $\theta$	h k l	d (Å)	FWHM (radians)	D (nm)	$\delta \times 10^{15}$ lines/m <sup>2</sup>	$\epsilon \times 10^{-3}$ lines/m <sup>2</sup>	SF $\times 10^{-3}$
0	32.84	2 0 2	2.73	5.307	27.255	1.346	1.272	3.239
	35.81	1 1 1	2.51	6.468	22.544	1.97	1.538	4.173
	38.91	1 1 1	2.31	3.979	36.980	73.1	0.938	2.716
	49.11	2 0 2	1.85	6.468	23.585	1.80	1.470	5.280
	53.79	0 2 0	1.7	6.468	24.054	1.73	1.441	5.742
	58.62	2 0 2	1.57	5.639	28.218	1.26	1.229	5.485
	61.86	1 1 3	1.5	5.639	28.685	1.22	1.209	5.856
	66.43	3 1 1	1.41	10.449	15.872	3.97	2.185	12.01
	68.51	1 1 3	1.37	9.288	18.073	3.06	1.919	11.243
0.05	32.67	0 0 2	2.74	10.447	13.842	5.22	2.506	6.356
	35.62	1 1 1	2.52	10.447	13.950	5.14	2.487	6.718
	38.78	1 1 1	2.32	11.61	12.670	6.23	2.737	7.906
	48.85	2 0 2	1.86	10.449	14.584	4.70	2.378	8.496
	53.44	0 2 0	1.71	16.584	9.367	0.114	3.702	14.623
	58.3	2 0 2	1.58	8.789	18.076	3.06	1.919	8.496
	61.66	1 1 3	1.5	13.268	12.179	6.74	2.848	13.72
	66.28	3 1 1	1.41	16.584	9.99	10.0	3.472	19.001
	68.18	1 1 3	1.38	11.61	14.431	4.80	2.404	13.938
0.1	32.62	0 0 2	2.74	6.468	22.351	2.00	1.552	3.931
	35.62	1 1 1	2.52	7.297	19.972	2.51	1.739	4.692
	38.78	1 1 1	2.32	8.459	17.3885	3.31	1.995	5.760
	48.9	2 0 2	1.86	7.627	19.9847	2.50	1.736	6.204
	53.64	0 2 0	1.71	11.276	13.788	5.26	2.516	9.98
	58.42	2 0 2	1.58	8.458	18.7957	2.83	1.846	8.195
	61.42	1 1 3	1.51	8.955	18.0216	3.08	1.929	9.217
	66.24	3 1 1	1.41	14.105	11.745	7.25	2.954	16.152
	68.28	1 1 3	1.37	8.458	19.8213	2.55	1.750	10.179

$$\delta = \frac{1}{D^2} \quad (2)$$

$$\epsilon = \frac{\lambda}{D \sin \theta} - \frac{\beta}{\tan \theta} \quad (3)$$

$$SF = \left[ \frac{2\pi^2}{45(3 \tan \theta)^2} \right] \beta \quad (4)$$

The defect factors of the  $\delta$ ,  $\epsilon$  and SF values were slightly increases with CTAB mole concentration, which indicates that increasing the oxygen vacancies in the CuO matrix [18].

## 3.2 SEM analysis

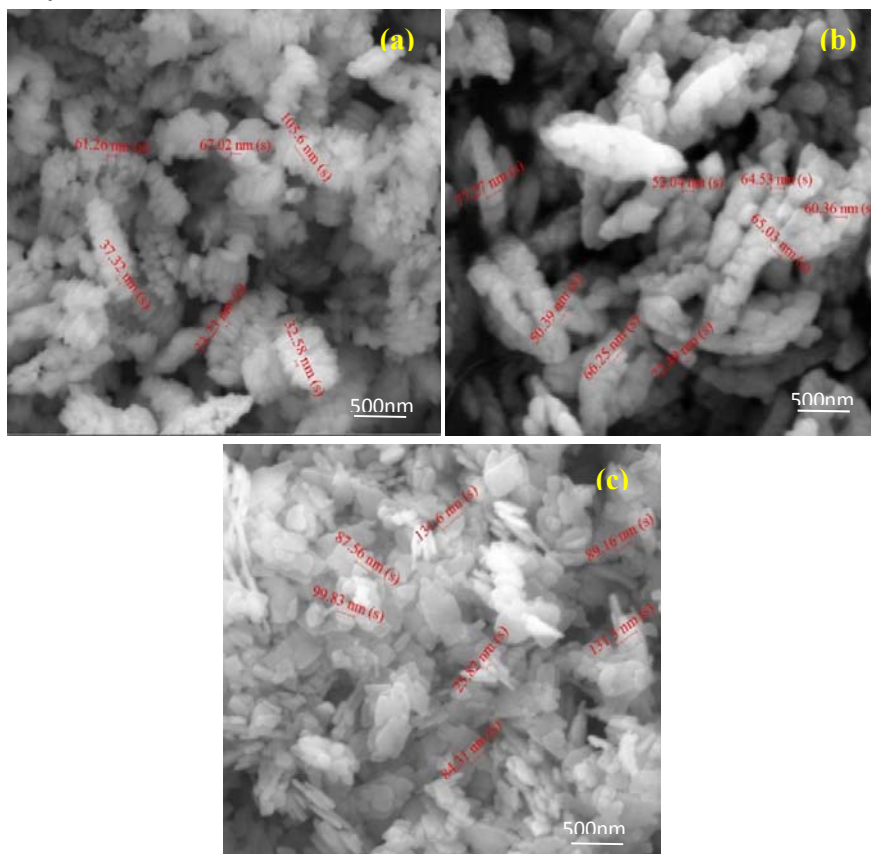


**Fig. 2(a-c)** SEM images of the CTAB assisted CuO NPs, (a) pure CuO NPs, (b) 0.05 M of CTAB:CuO NPs and (c) 0.1 M of CTAB:CuO NPs.

The SEM images of the pure and CTAB assisted CuONPs is shown in Fig. 2(a-c). Fig. 2(a) shows that the sponge-like nano sized grains are observed. The 0.05 M of CTAB assisted CuO NPs surface morphology shows that well agglomerated needle-like grain structures (Fig. 2(b)). From the Fig. 2(c), nano sized plate-like structures for 0.1 M of CTAB assisted CuO NPs.

This results indicates that the CTAB is strongly influences on the surface morphology and grain size of the CuO NPs. EDX spectra of uncapped CuO and different surfactant assisted CuO NPs shown in Fig. 3(a-c). EDX spectra results indicated the presence of Cu and O elements. The atomic ratio of the Cu and O elements listed in table 2.

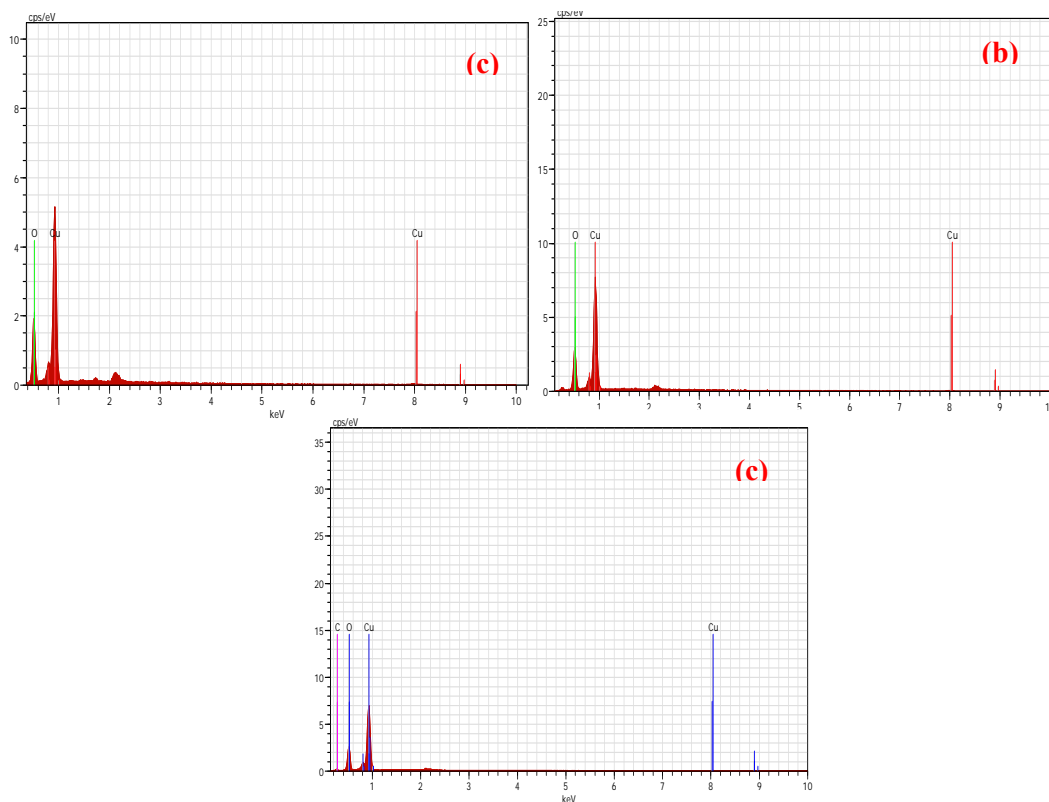


**Fig. 3(a-c)** EDX spectra of the CTAB assisted CuO NPs, (a) pure CuO NPs, (b) 0.05 M of CTAB:CuO NPs and (c) 0.1 M of CTAB:CuO NPs.

**Table 2:** Atomic ratio of the CuO NPs

Atomic%	Pure CuO NPs	CTAB(0.05 M):CuO NPs	CTAB(0.1M):CuO NPs
<b>Cu</b>	52.59	51.12	53.39
<b>O</b>	47.41	48.88	47.61

### 3.3 UV-visible analysis

Fig. 4(a-c) shows UV-visible spectra of the CuO NPs analysed by diffuse reflectance (DR) mode. The absorbance spectra of the prepared NPs reveals a higher absorbance value

obtained for 0.05 M of CTAB assisted CuO NPs as shown in Fig. 4(b).

The absorption coefficient is found from reflectance data (DRS mode) by using Kubelka-Munk relation [19]

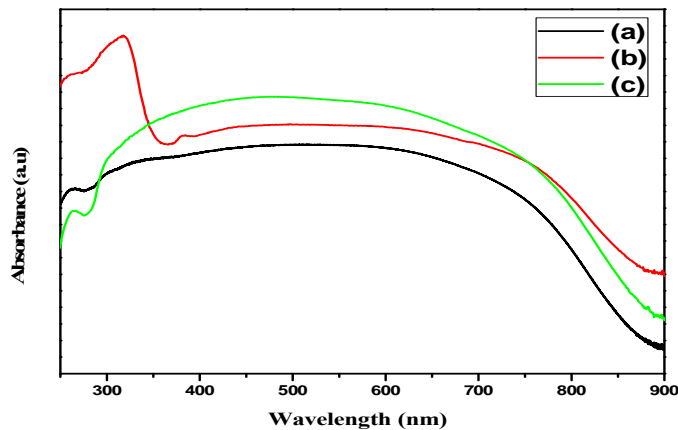


**Fig. 4(a-c)** optical absorbance spectra of the CTAB assisted CuO NPs, (a) pure CuO NPs, (b) 0.05 M of CTAB:CuO NPs and (c) 0.1 M of CTAB:CuO NPs.

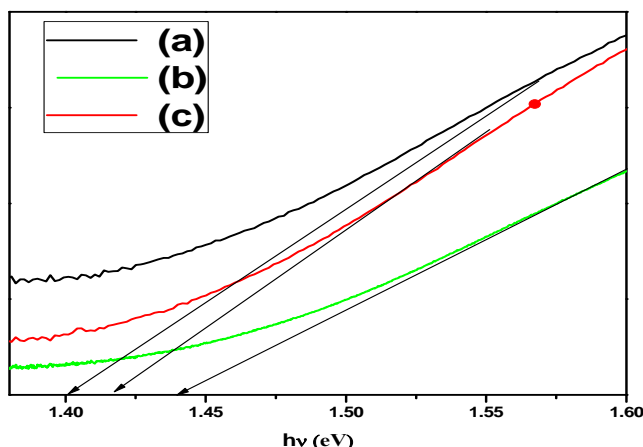


Fig. 5(a-c) band gap spectra of the CTAB assisted CuO NPs, (a) pure CuO NPs, (b) 0.05 M of CTAB:CuO NPs and (c) 0.1 M of CTAB:CuO NPs

$$KMU = (1-R)^2/2R \quad (5)$$

where  $R$  is reflectance. The band gap ( $E_g$ ) is determined by the square root of Kubelka–Munk function multiplied by the photon energy  $(\alpha hv)^{1/2}$  is plotted against photo energy ( $h\nu$ ) as shown in Fig. 5(a-c). The band gap value was calculated from the Kubelka-Monk method. The band gap energy is found 1.40 eV, 1.42 eV and 1.46 eV for pure, 0.05 and

0.1 CuO NPs, respectively [20]. The band gap increased with incorporation of the CTAB, which denotes that quantum confinement effect.

### 3.4 Dc electrical analysis

The dc electrical characteristics of the CTAB assisted CuO NPs as a function of temperature in the range of 29-100 °C is shown in fig.6(a-d).

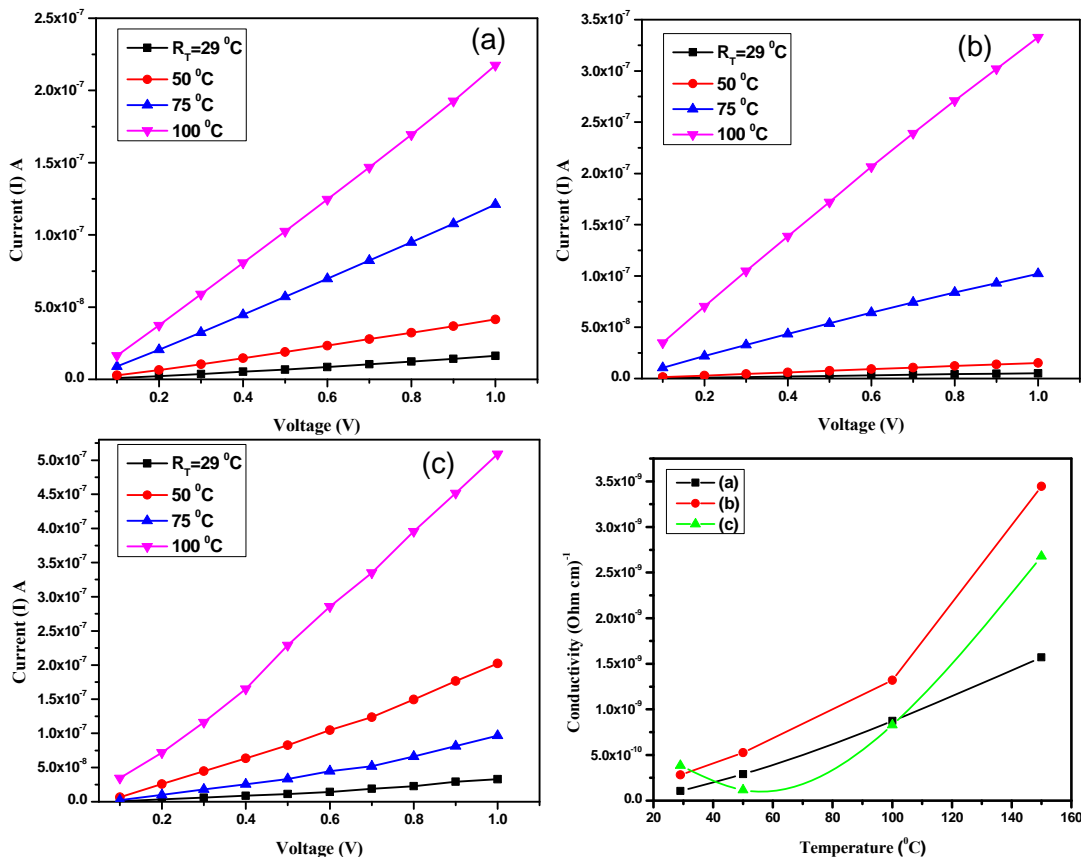


Fig. 6(a-d) I-V characteristics of the CTAB assisted CuO NPs, (a) pure CuO NPs, (b) 0.05 M of CTAB:CuO NPs and (c) 0.1 M of CTAB:CuO NPs and 5(d) temperature dependence of electrical conductivity of the prepared NPs.

From the figure 6(a-c), linear variation of the current-voltage (I-V) curve indicates that the ohmic behavior of the prepared NPs. The electrical conductivity is calculated using the expression of  $\sigma = \frac{t}{RA}(\Omega \text{ cm})^{-1}$ . Fig. 6(d) shows the conductivity increases with temperature reveals that the semiconducting nature of CuO NPs. The higher conductivity ( $\sigma_{dc}$ ) was obtained for 0.05 M of CTAB assisted CuO NPs.

### 3.5 Diode characteristics

The p-CuO/n-Si junction diodes were characterized by I-V measurement as a function of temperature in dark at room temperature ( $R_T = 302 \text{ K}$ ) for 0.05 M of CTAB assisted CuO NPs. I-V characterization of the p-CuO/n-Si junction diodes is expressed in terms of thermionic emission (TE) model [21],

$$I = I_0 \left[ \exp\left(\frac{qV}{nk_B T}\right) - 1 \right] \quad (11)$$

where  $q$  is the elementary charge,  $K_B$  is the Boltzmann constant,  $n$  is the ideality factor,  $T$  is the absolute temperature in Kelvin,  $I_0$  is the reverse leakage current and  $V$  is the applied bias. The  $I_0$  is calculated using the following expression

$$I_0 = AA^* T^2 \exp\left(\frac{-q\Phi_B}{k_B T}\right) \quad (12)$$

where  $\Phi_B$  is effective barrier height at  $V = 0$  and  $A^*$  is the Richardson constant ( $110 \text{ A/cm}^2 \text{K}^{-2}$  for n-type silicon).

The ideality factor ( $n$ ) and barrier height ( $\Phi_B$ ) were determined by the fabricated device using the following relations

$$n = \frac{q}{k_B T} \left( \frac{dV}{d \ln(I)} \right) \quad (13)$$

$$\Phi_B = \frac{k_B T}{q} \ln\left(\frac{A^* T^2}{I_0}\right) \quad (14)$$

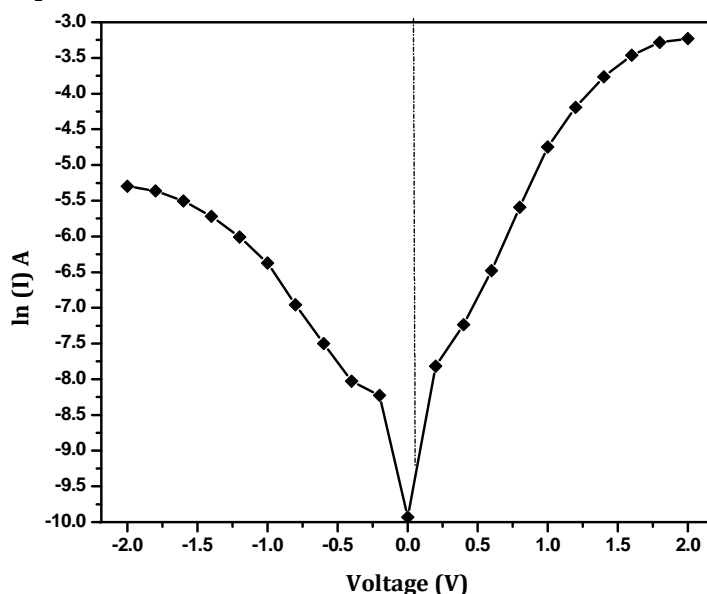


**Fig. 7(a-d)**  $\ln(I)$ -V characteristics of the CTAB assisted p-CuO NPs/n-Si diode.

Fig. 7 shows the semi-logarithmic plot of  $\ln(I)$ -V for the pure and the annealed devices (73K-773K). The  $n$  and  $\Phi_B$  are determined from the y-slope and the intercept of the fitted curve, respectively. From the forward bias  $\ln(I)$ -V plot, the diode parameters of  $I_0$ ,  $n$ , and  $\Phi_B$  values are 4.25, 0.82 and  $9.21 \times 10^{-10} \text{ A}$ , respectively.

### 4. Conclusion

The structural, optical and dc electrical properties of CuO NPs was investigated by varying mole concentration of the CTAB. The XRD analysis shows the tetragonal structures the  $D$  values varied from 2.21 to 3.18 nm for the predominant peak (1 1 0) of CuO NPs. The CuO

NPs consist of nano sized sponge and plate-like grains, which induce grain growth and uniform agglomeration on the surface. The 0.05 M of CTAB assisted CuO NPs showed that a higher conductivity ( $\sigma_{dc}$ ) due to with rising oxygen deficiency. The 0.05 M of CTAB assisted p-CuO/n-Si junction diodes of  $n$ ,  $\Phi_B$  and  $I_0$  with values of 4.25, 0.82 and  $9.21 \times 10^{-10} \text{ A}$ , respectively.

### Acknowledgement

The author would like to acknowledge DST FIST UGC SAP, DST PURSE for the instrumental facilities available in the department of Nano Science and Technology, Bharathiar University, Coimbatore.

**References**

- [1] Luo,L.B.; Wang,X.H.;Xie,C.; Li,Z.J.; Lu,R.; Yang,X.B.; Lu,J.; *Nanoscale Res. Lett.*, **2014**, 9, 637.
- [2] Li, C.; Yang, X.G.;Yang, B.J.;Yan, Y.;Qian, Y.T.;*Eur. J. Inorg. Chem.*,**2003**,19, 3534–3537.
- [3] Li, Y.M.;Liang, J.; Tao, Z.L.;ChenJ.; *Mater. Res. Bull.*,**2008**,43,2380-2385.
- [4] Zhang, Z.L.;Chen, H.;Che, H.W.; Wang, Y.H.;Su, F.B.;*Mater. Chem. Phys.*, **2013**,138 593-600.
- [5] Alireza, N.E.;Shohreh, H.;*Appl. Catal., A: Gen.*, **2010**, 388,149-159.
- [6] Meshram, S.P.;Adhyapak, P.V.;Mulik, U.P.;Amalnerkar, D.P.;*Chem. Eng. J.*,**2012**,204-206,158-168.
- [7] Dubal, D.P.;Dhawale, D.S.;Salunkhe, R.R.;Jamdade, V.S.;Lokhande, C.D.;*J. Alloy Compd.*,**2010**,492, 26-30.
- [8] Lin, X.;Liang, J.;Kishi, N.;Soga, T.; *Mater. Lett.* **2013**, 96, 192–194.
- [9] Siddiqui, H.;Qureshi, M.S.;Haque, F.Z.;*Optik***2016**,127,2740–2747.
- [10] Zou, Y.;Li, Y.; Zhang, N.; Liu, X.;*Bull. Mater. Sci.*, **2011**,34,967–971.
- [11] Reddy,S.; Kumara Swamy,B.E.;Jayadevappa, H.; *Electrochim. Acta*,**2012**, 61, 78–86
- [12] Wang, S.;Xu, H.; Qian, L.;Jia, X.;Wang, J.;Liu, Y.; Tang, W.;*J. Solid State Chem.*, **2009**, 182,1088–1093.
- [13] Zhu, J.;Li, D.;Chen, H.;Yang, X.;Lu, L.;Wang, X.;*Mater. Lett.*, **2004**, 58,3324-3327.
- [14] Jang, J.; Chung, S.;Kang, H.;Subramanian, V.;*Thin Solid Films* **2016**,600,157-161.
- [15] Ghosh, M.; Rao, C.N.R.;*Chem. Phys. Lett.*,**2004**,393, 493.
- [16] Wang, X.; Yang, J.; Shi, L.; Gao, M.; *Nanoscale Res. Lett.*, **2016**, 11,125-132.
- [17] Punnoose , A.;MagnoneA.;Seehra, M.S.;*Phys. Rev. B.*,**2001**, 64, 14120,
- [18] Aygun, S.; Cann, D.;*Sens. Actuators B*, **2005**, 106,837–842.
- [19] Lin, K.F.;Cheng, H.M.;Hsu, H.C.;Lin, L.J.;Hsieh, W.F.;*Chem. Phys. Lett.*,**2005**, 409,208-211.
- [20] Siddiqui, H.;Qureshi, M.S.;Haque, F.Z.;*Optik***2014**, 125,4663–4667.
- [21] SzeS.M.; *Physics of Semiconductor Devices*, John Wiley and Sons, New York, 1981.